THE ASTROPHYSICAL JOURNAL, 409:155–161, 1993 May 20

X-RAY EVIDENCE FOR SEYFERT ACTIVITY BURIED IN THE INFRARED GALAXY NGC 4945

K. IWASAWA,[1] K. KOYAMA,[2] H. AWAKI,[1] H. KUNIEDA,[1] K. MAKISHIMA,[3] T. TSURU,[2]
T. OHASHI,[3] AND N. NAKAI[4]

Received 1992 April 10; accepted 1992 November 16

ABSTRACT

We have observed the infrared galaxy NGC 4945 using the Japanese X-ray astronomy satellite, *Ginga*. The X-ray spectrum is found to be composed of three components: hard X-ray emission which is heavily absorbed by cold material with column density of about $10^{24.7}$ cm^{-2}; a soft X-ray component seen in the 2–10 keV band; and an iron emission line. The hard component exhibits a power-law spectrum with photon index of about 1.7. The mean X-ray luminosity in the 2–20 keV band, after correction for absorption is 3×10^{42} ergs s^{-1} with significant intensity variation on a time scale of several hours. These results are thought to be evidence for an AGN (active galactic nucleus) in the galaxy. The X-ray spectrum of the soft component can be fitted with a power-law model having nearly the same photon index, but the luminosity is only 3% that of the hard component. The soft component shows no time variability. The energy of the iron line is found to be 6.5 ± 0.1 keV, and the equivalent width is 1.5 ± 0.3 keV. The X-ray spectrum is interpreted to be composed of the X-ray emission from a hidden Seyfert nucleus behind an obscuring torus, the scattered continuum radiation, and a fluorescence line emission from ionized iron in the scattering medium. Thus NGC 4945 is the first example of an active galaxy which exhibits both *the obscuring and scattering picture* of the type 2 AGN.

Subject headings: galaxies: individual (NGC 4945) — galaxies: nuclei — galaxies: Seyfert — X-rays: galaxies

1. INTRODUCTION

NGC 4945 is an edge-on spiral galaxy in the southern hemisphere at a distance of 6.7 Mpc (Whiteoak & Gardner 1977). Strong extinction in the dusty plane of the edge-on galaxy has prevented detailed study at visual wavelengths, particularly in the blue region.

This galaxy has a bright compact core which shows activity in a wide range of wavelength. Strong and compact power-law ($F_\nu \propto \nu^{-0.6}$) radio emission is present in the central part, and the position is coincident with the peak of optical and infrared emission (Harnett & Reynolds 1985).

Whiteoak & Gardner (1979) reported the presence of a broad forbidden line with velocity larger than 600 km s^{-1}, and the intensity ratio of [N II]λ6583 to Hα was found to be about 3. The near-infrared emission-line spectra indicate strong emission of molecular hydrogen (H_2) relative to the Brγ recombination emission line (Moorwood & Oliva 1988). Statistical studies of Seyfert galaxies and starburst galaxies have shown that active galactic nuclei (AGNs) are a major source of H_2 excitation (Heckman et al. 1986; Kawara, Nishida, & Gregory 1990).

NGC 4945 is the third brightest galaxy in the *IRAS* Point Source Catalog with a far-infrared luminosity of 8×10^{43} ergs s^{-1}. The *IRAS* and the KAO (the Kuiper Airborne Observatory) scan profiles shown by Rice et al. (1988) and Brock et al. (1988), respectively, have demonstrated that the infrared emission arises predominantly from the central compact region. While these infrared results alone seem to show starburst activity, Brock et al. (1988) suggested that the infrared emission could be powered by a compact nonstellar source, such as a type 2 Seyfert or low-ionization nuclear emission-line region (LINER).

Several strong molecular absorption lines have been detected in the nuclear region. Abels et al. (1987) found from study of H I that the absorbing clouds are located within a few hundred pc of the nucleus. Brock et al. (1988) found the lower limit of the 100 μm optical depth to be $\tau_{100\mu m} \geq 0.35$, corresponding to $A_v \geq 175$. This extremely large value is consistent with the optical depth at 10 μm being due to the silicate absorption derived by Moorwood & Glass (1984). Thus the nucleus seems to be deeply embedded in a dust cloud.

NGC 4945 has been found to exhibit starburst activity including a large infrared luminosity and *IRAS* color similar to a giant H II region. A large "hollow cone" feature (2×10 kpc) in the broad-band optical image suggesting outflowing gas from the nuclear region was found by Nakai (1989). The double-peaked optical emission-line profiles were discovered along the minor axis of the galaxy; this is inferred as evidence for a superwind (Heckman, Armus, & Miley 1990). They interpreted this evidence to imply that NGC 4945 has a galactic superwind driven by starburst activity, because of its similarity to well-known starburst galaxies, M82 and NGC 253. NGC 4945 is also a most luminous source of H_2O maser emission ($\sim 200\ L_\odot$), rarely found in extragalactic objects (dos Santos & Lepine 1979; Bachelor, Jauncey, & Whiteoak 1982; Baan 1985; Whiteoak & Gardner 1986).

Although a number of observations are available from various wavelengths, no X-ray observation has been conducted so far. X-ray observations, in particular in the hard X-ray band, are crucial for the investigation of the activity of NGC 4945, because the X-ray emission may be directly attributed to the AGN activity and the thick dusty clouds around the nucleus may be transparent to hard X-rays. We present results of the *Ginga* observations of NGC 4945 and discuss the nature of the nuclear activity of NGC 4945. In this paper, the distance of NGC 4945 is assumed to be 6.7 Mpc.

[1] Department of Astrophysics, Nagoya University, Furo-cho, Chikusa-ku, Nagoya 464-01, Japan.
[2] Department of Physics, Kyoto University, Sakyo-ku, Kyoto 606-01, Japan.
[3] Department of Physics, University of Tokyo, Hongo, Bunkyo-ku, Tokyo 113, Japan.
[4] Nobeyama Radio Observatory, National Astronomical Observatory, Minamimaki-mura, Minamisaku-gun, Nagano 384-13, Japan.

2. OBSERVATIONS

NGC 4945 was observed with the *Ginga* LAC (Large Area Proportional Counter; Turner et al. 1989) on 1990 July 24 pointing at the position of (α, δ) = (195.63, −49.20). An unidentified *HEAO 1* source 1H 1304−497 (Wood et al. 1984) is located close to NGC 4945, and no *Einstein* IPC observation was performed near this region. Therefore, in order to resolve any confusion of X-ray emission from possible contaminating sources, scanning observations over the NGC 4945 region were made on 1990 July 25 from one direction (path 1) and on 1991 June 24 from another direction (path 2). The scan paths are shown in Figure 1 together with the LAC field of view (FOV) during the pointing observation. As is shown in Figure 1, the crossing angle of the two scan paths is approximately 30°. On path 1 and path 2, four and six consecutive scans, respectively, were performed. The LAC response for a point source has an approximately triangular shape with 1° FWHM (Turner et al. 1989). The scan speeds of the two observations were 0.°4 minute^{-1} and 0.°5 minute^{-1}, respectively.

The 1–37 keV data were accumulated into 48 pulse-height channels (MPC-1 mode) with low bit rate providing a time resolution of 16 s. Since the X-ray flux of NGC 4945 is low, in order to obtain reliable X-ray data, the data selection was made carefully. The data accumulated in the ground-contact orbits were excluded because of the higher background level due to the South Atlantic Anomaly. The data from the regions of low geomagnetic cutoff rigidity (<9 GeV c^{-1}) and unusual high background events due to sudden increases in the charged particle flux were also excluded (Hayashida et al. 1989; Awaki 1991). The effective accumulation time of useful data in the pointing mode was 1 × 10^4 s.

Observed raw data include the internal background (non–X-ray background) of the LAC experiment (IBG) and the cosmic diffuse X-ray background (CXB) as well as the source flux. The behavior of the IBG has been investigated by Hayashida et al. (1989) and Awaki et al. (1990a). We estimated the IBG for the present observations using the method developed by Awaki (1991). The CXB spectrum was made by adding nine blank sky spectra which were obtained during the period from 1990 June to 1990 August, at high galactic latitude free from the Galactic ridge emission. Total exposure time of the background data is 5 × 10^4 s, which is significantly longer than that of the on-source observation. A local CXB spectrum near NGC 4945 was constructed from this mean CXB spectrum by normalizing the total flux to that of the nearby sky.

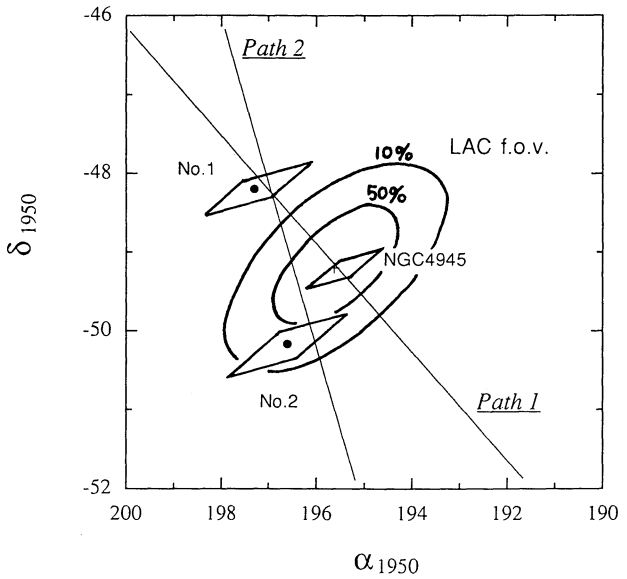

FIG. 1.—Sky map of the NGC 4945 region. Scan path 1 and 2, on which the center of the LAC FOV passed through, are shown in solid lines. The scan path 1 passes over NGC 4945. The scan path 2 is offset 0.°64 to West of NGC 4945. Error boxes of the two unidentified sources (no. 1, no. 2) are deduced from the two projected positions with its 90% confidence errors onto the two scan paths using the results of convolution fitting for the scan profiles (Table 1B). The LAC FOV during the pointing observation is also shown in contours by which 50% and 10% of transmission efficiency of the LACs collimator are shown.

3. RESULTS AND ANALYSIS

3.1. *Scan Profiles*

In Figures 2*a* and 2*b*, we present the folded scan profiles obtained in 1.7–5.1 keV and 5.1–30 keV ranges on the scan paths 1 and 2, respectively. The center of the scan profiles (scan angle = 0°) corresponds to the projected optical position of NGC 4945. In the hard X-ray band, the scan profiles show a single peak near the center, which seems to coincide with the position of NGC 4945. On the other hand, the soft X-ray profiles show more complicated structure, possibly due to multiple sources in the vicinity of NGC 4945. Thus, at first we tried convolution fits to the hard X-ray profiles near the center assuming one point source. Free parameters were position and intensity of the source. The fits were acceptable and the results are given in Table 1A. The 90% error region of the central source includes the position of NGC 4945. In fact, we obtained acceptable fits by fixing the source position at 0°, as illustrated in Figures 2*a* and 2*b*. Thus we conclude that the hard X-ray source at the center originates from NGC 4945. The hard X-ray fluxes determined from scan profiles on paths 1 and 2 are different from one another, suggesting that NGC 4945 is time variable in the hard X-ray band.

Next, we applied a similar fitting procedure to the soft X-ray profiles. Since the scan profiles near the center are complicated, we fixed the position of the central source (NGC 4945) to be at 0°. In path 2, the intensity of NGC 4945, and the positions and intensity of two other contaminating sources were left as free parameters. In order to obtain an acceptable fit, we need at least two new sources other than NGC 4945, as illustrated in Figure 2*b*. In path 1, we assumed that the intensity of NGC 4945 is equal to that determined with the path 2 fitting, because we find that the soft X-ray flux of NGC 4945 shows no time variability, as is demonstrated in the next section. We also need two sources to obtain an acceptable fit, as shown in Figure 2*a*. The best-fit results are given in Table 1B and the 90% error regions of the two new sources are shown in Figure 1.

In order to discover information about the spectra of these new sources, we made scan profile fittings in the energy bands of 1.7–2.8 keV and 2.8–5.1 keV and obtained fluxes from each. From the flux ratios of the two energy bands, we derive temperatures, assuming a thermal bremsstrahlung emission. The results are summarized in Table 1C.

3.2. *Pointing Data*

The X-ray spectrum acquired during the pointing observation is shown in Figure 3. The hard X-ray flux in the 5.1–30 keV range is 3 counts s^{-1}, which is in good agreement with the

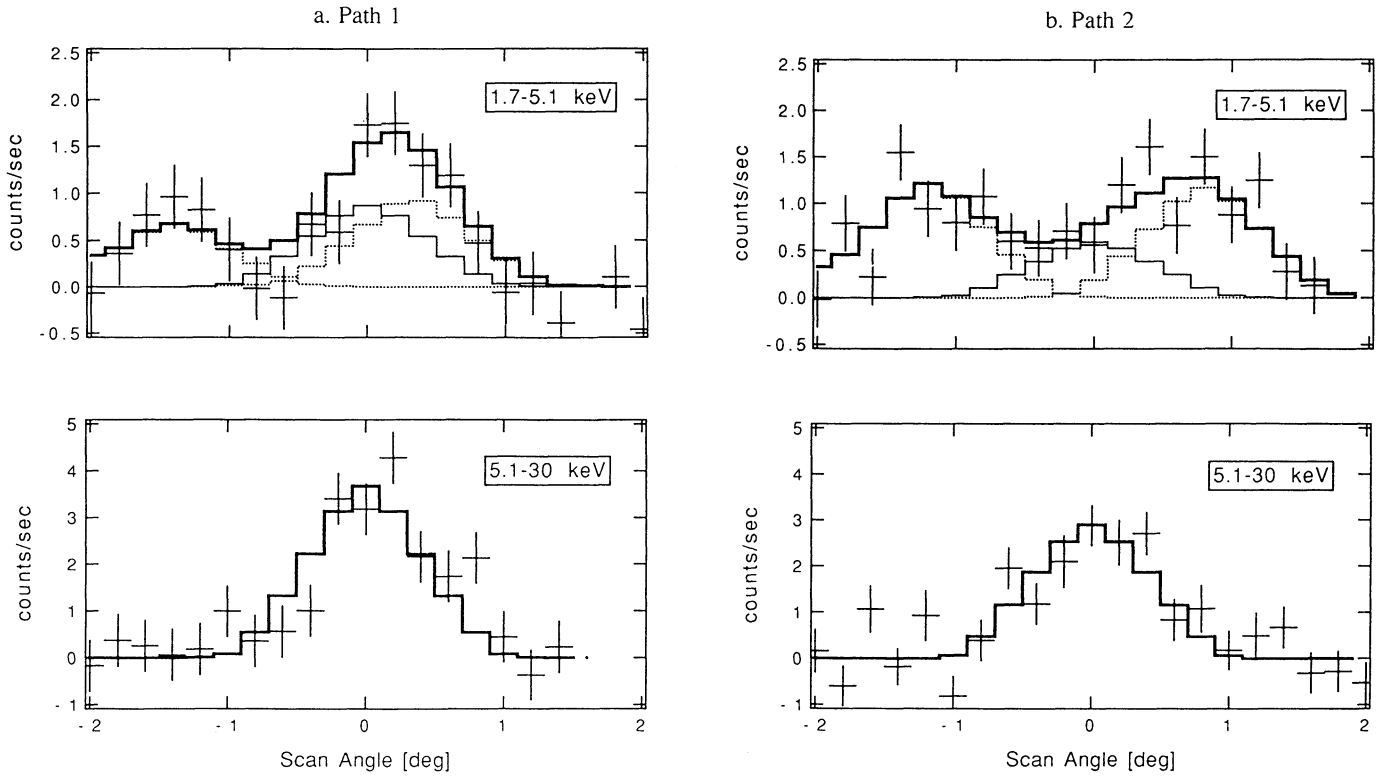

FIG. 2.—Scan profiles along the path 1 (*a*) and the path 2 (*b*) in the 1.7–5.1 keV and 5.1–30 keV band. The center of the profiles (scan angle = 0°) corresponds to the projected position of NGC 4945. Crosses are data points of count rate with angular resolution of 0°2. In the profile of the 1.7–5.1 keV band, thin lines show each model profile of X-ray sources listed in Table 1B; from left: source no. 1 (*dotted line*), NGC 4945 (*solid line*), and source no. 2 (*dotted line*); and thick solid line shows the integration of them.

results obtained from the scan profile 1. The first scanning observation was carried out on the day after the pointing observation. Since a new source (no. 2) was in the LAC FOV during the pointing observation, we estimate the contribution of this source using the spectral parameters determined from the scan observations. The estimated contribution is shown by the dotted line histogram in Figure 3, where we adopt the temperature and X-ray flux (2–10 keV band) to be $kT \sim 3$ keV and 1×10^{-12} ergs cm^{-2} s^{-1}, respectively. The effect on the spectral subtraction due to the uncertainties on the parameters of the contaminating source is discussed later in this section.

The X-ray spectrum of NGC 4945 has an excess above 10 keV and an intense iron emission line. Obviously the spectral shape cannot be described with a single component model but needs at least a two-component continuum with an emission line. Thus we performed the spectral fitting using a two-component power-law continuum, modified for the effects of absorption due to cold gas, and an iron emission line, in the energy range of 3–30 keV. The interstellar absorption cross sections were taken from Morrison & McCammon (1983). Since the new source no. 2 contributes significantly at low energies below about 5 keV, we disregarded this energy band for the following fits. The power-law slope of two components were at first fitted independently (model 1). Model 1 was acceptable, as shown in Table 2, but within 1 σ errors we find that the two best-fit power-law indices are consistent with one another. Accordingly we tried a simpler model in which the two continuum-components have a common slope (model 2). The fitting is equally acceptable as is summarized in Table 2 and illustrated in Figure 3.

In either model, the absorption column density of the hard component is found to be extremely large (log $N_{\rm H} = 24.73 \pm 0.04$ cm^{-2}). The energy and equivalent width of the emission

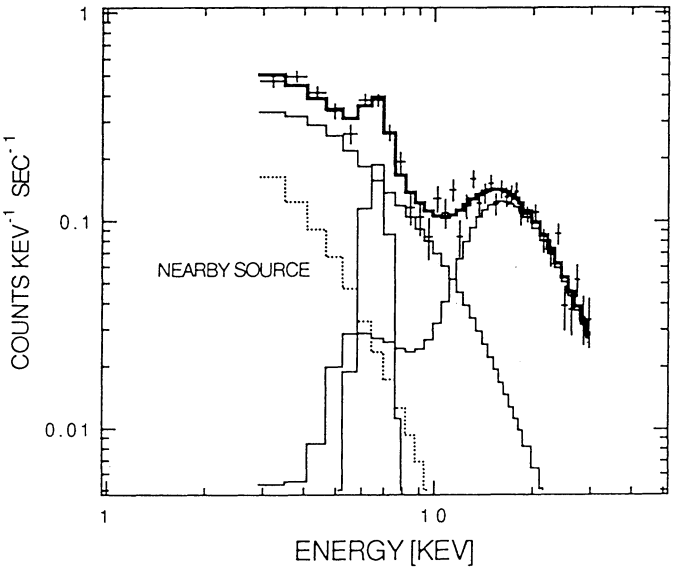

FIG. 3.—*Ginga* count rate spectrum of NGC 4945 in the 3–30 keV range. Deduced energy spectrum of the nearby source (no. 2; see text) is also shown in the histogram of the dotted line. Best-fit two-component absorbed power-law model and an iron emission line (model 2: see text) are shown in histograms of solid line (of which each component is shown in thin line and the sum in thick line).

TABLE 1

RESULTS OF SCANNING OBSERVATIONS

A. COUNT RATE AND AZIMUTHAL ANGLE (5.1–30 keV)

Scan Path	Count Rate	Az.	χ^2 (dof)
Path 1.....	3.0 (0.5)	0.10 (0.1)	44 (23)
Path 2.....	4.4 (0.8)	0.07 (0.1)	42 (23)

NOTE.—Count rate and azimuthal angles are in units of counts per second and degree, respectively. Correction for the transmission efficiency of the LAC FOV in the direction of its major axis caused by off-set of the path 2 from NGC 4945 was done. The χ^2 values together with degrees of freedom are given for the best-fit parameters. Errors at 90% confidence level are shown in parentheses.

B. COUNT RATE AND AZIMUTHAL ANGLE (1.7–5.1 keV)

	NGC 4945		No. 1		No. 2		
SCAN PATH	Count Rate	Az.	Count Rate	Az.	Count Rate	Az.	χ^2(dof)
Path 1.....	0.9 (fixed)	0	0.7 (0.3)	−1.4 (0.2)	1.0 (0.3)	0.3 (0.2)	34 (21)
Path 2.....	0.9 (0.6)	0	1.2 (0.3)	−1.2 (0.1)	1.2 (0.3)	0.8 (0.2)	40 (20)

NOTE.—Count rate and azimuthal angles are in unit of counts per second and degree, respectively. Errors at 90% confidence level are shown in parentheses. Count rate of NGC 4945 on the path 1 is fixed at value obtained from path 2 in relevant fitting procedure (see text).

C. SPECTRAL INFORMATION OF THE TWO NEARBY SOURCES

Source	L/H[a]	kT[b]
No. 1.....	1.0 (0.4)	$2.1^{+2}_{-0.7}$
No. 2.....	0.8 (0.4)	$3.0^{+5.5}_{-1.3}$

[a] L/H: *Ginga* count rate ratio in 1.7–2.8 keV range relative to in 2.8–5.1 keV range.

[b] kT: deduced temperature from L/H assuming a thermal bremsstrahlung emission model. Errors of higher bound of the temperature are estimated from upper limits of the count rate above 5.1 keV band.

line are found to be 6.5 ± 0.1 keV and 1.5 ± 0.3 keV, respectively.

Although the extremely large column is completely opaque to X-rays below 10 keV, we estimate the *intrinsic* X-ray luminosity of the hard components in the 2–10 keV energy range to be 1×10^{42} ergs s^{-1}, assuming the best-fit power-law index of 1.7. The X-ray luminosity of the soft component is estimated to be 3×10^{40} ergs s^{-1} in the 2–10keV range. As a result, the luminosity of the soft X-ray component is only $\sim 3\%$ of that of the hard component.

We estimated the effect of contamination due to the X-ray source no. 2, considering the errors on the spectral parameters listed in Table 1C. The fittings were made using model 1 and fixing parameters of the hard component to the best-fit values listed in Table 2. In this case the low-energy data below 3 keV were included. We found that the uncertainties of Γ, log N_H, and $L_{x,40}$ (2–10 keV band in units of 10^{40} ergs s^{-1}) are in the range of 1.2–1.9, <22.6, and 1.5–3.4, respectively.

Interruption by the Earth occultation and high background regions during the orbital motion of *Ginga* satellite cause the

TABLE 2

SPECTRAL FIT TO THE X-RAY SPECTRUM OF NGC 4945

	HARD COMPONENT		SOFT COMPONENT		Fe LINE		
MODEL	Photon Index	log N_H (H cm^{-2})	Photon Index	log N_H (H cm^{-2})	E_{center} (keV)	EW (keV)	REDUCED χ^2 (DOF)
(1).....	1.5 ± 0.3	24.70 ± 0.06	1.8 ± 0.3	22.37 ± 0.64	6.5 ± 0.1	1.5 ± 0.3	1.3 (30)
(2).....	1.7 ± 0.1*	24.73 ± 0.04	1.7 ± 0.1*	22.16 ± 0.56	6.5 ± 0.1	1.5 ± 0.3	1.3 (29)

NOTE.—Errors indicate 90% confidence region. In model (1), both photon indices are free parameters, while in model (2), a common photon index* is adopted for the two components in the fitting. EW indicates equivalent width of the iron emission line against the continuum of the soft component.

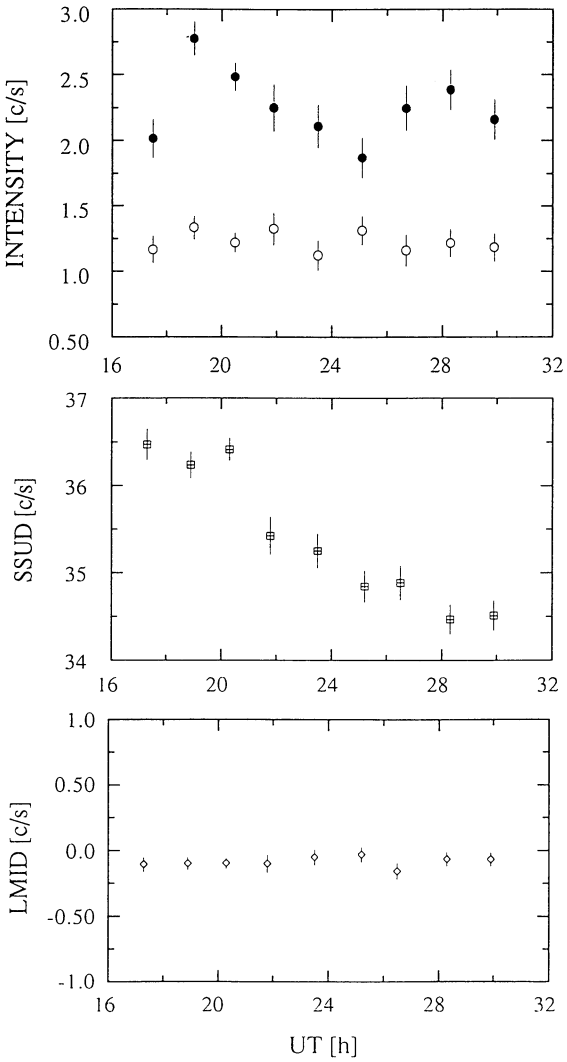

FIG. 4.—(*a*) X-ray light curves of NGC 4945 during the pointing observation. Count rate in the 4.5–9.1 keV (*open circles*) and that in the 9.1–30 keV (*filled circles*) are shown. (*b*) Plot of the SSUD count rate during the same period in the observing run. The SSUD count rate is well correlated with internal background of the LAC experiment (non–X-ray background). The internal background decreases almost monotonically. (*c*) Plot of the count rate from the MID layer of the LAC in the 2–6 keV range (LMID). If non–X-ray background is properly subtracted, these are nearly zero because the MID layer is insensitive to this energy range. As you see in this plot, the internal background of the LAC is found to be properly subtracted for this observation.

pointed data to be divided into several subgroups, each with an accumulation time of about 10^3 s. Figure 4 shows light curves from the two energy bands with a time resolution of 10^3 s. From the spectrum in Figure 3, we note that the lowest energy band (4.5–9.1 keV) is dominated by the soft component, while the high-energy band (9.1–30 keV) is dominated by the hard component. To avoid the contribution from the nearby new soft X-ray source, the low-energy flux below 4.5 keV was not used in the light curve. The averaged intensity of the hard X-ray band is 2.3 counts s^{-1}, with significant intensity variation on a time scale of several hours. In fact, the constant intensity hypothesis is rejected at more than 99% confidence level (reduced χ^2 is 3.9 for 8 degrees of freedom). To check whether this intensity variation is instrumental or not, we made a plot of super surplus over upper discrimination (SSUD) count rate (Hayashida et al. 1989) as a function of time during this period, since SSUD shows good correlation with the internal background of the LAC instrument (Hayashida et al. 1989; Awaki et al. 1990b). As is shown in Figure 4, the SSUD count rate did not show a random but rather a smooth variation. Thus we find no correlation between the hard X-ray variability of NGC 4945 and the LAC background. Furthermore we have checked the background-subtracted middle (MID) layer counts in 2–6 keV band. In this band, the MID layer has less than 1% sensitivity for X-ray photons. Since the count rate in this band was nearly zero as shown in Figure 4, the background should have been properly subtracted. Thus we conclude that the derived light curve is reliable and hence the intensity variation of the hard X-rays is real.

On the other hand, the X-ray flux in the soft band shows no significant variation (reduced χ^2 is 0.54 for 8 degrees of freedom), with the average intensity of 1.2 counts s^{-1}.

4. DISCUSSION

4.1. *X-Ray Evidence for a Heavily Obscured AGN*

The *Ginga* X-ray spectrum of NGC 4945 has a two-component continuum which consists of a strongly absorbed hard X-ray component and a less-absorbed soft component. The spectral slope for both components is $\Gamma \sim 1.7$, which is similar to the typical value found in Seyfert galaxies (Mushotzky 1982; Rothschild et al. 1983). The hard X-ray component shows intensity variation on a time scale of a few hours. Intrinsic X-ray luminosity of the hard component corrected for absorption is estimated to be 1×10^{42} ergs s^{-1} in the 2–10 keV band. This value is nearly equal to the lower bound of Seyfert galaxies but larger than that of the most luminous of starburst galaxies (cf. Weedman et al. 1981; Phillips, Charles, & Baldwin 1983).

Furthermore we find time variability in the hard X-ray band. The amplitude of the variability is 20%–25% compared with the averaged intensity. The doubling time (Barr & Mushotzky 1986) is $\sim$9 hr. X-ray variability on such a short time scale suggests the existence of a compact X-ray emitter in NGC 4945. The time scale of the variation is $\sim 10^4$ s giving an upper limit on the size of the X-ray emitter of $\sim 10^{15}$ cm, using the light crossing time to determine the size of the emitting region. Thus the hard X-ray component suggests that NGC 4945 has a compact nonthermal source, like a Seyfert 1 nucleus.

We find that the low-energy absorption of the hard X-ray component is extremely large with $N_H \sim 10^{24.7}$ cm^{-2}. There have been found several absorption lines of H I (Whiteoak & Gardner 1976), OH (Whiteoak & Gardner 1973) and H_2CO (Gardner & Whiteoak 1974) implying that a substantial amount of molecular cloud are located near the nucleus. The H I absorption measurement implies that the molecular absorbing clouds are located within a few hundred pc of the nucleus (Abels et al. 1987). Brock et al. (1988) measured the 100 μm optical depth to be ≥ 0.35, corresponding to a visual extinction $A_V \geq 175$. This gives an absorption column of about 3×10^{23} cm^{-2}, using the standard gas-to-dust ratio. The optical depth of 10 μm due to the silicate absorption is larger than 4 (Moorwood & Glass 1984), corresponding to N_H of 10^{23} cm^{-2}. The present X-ray measurement gives a more precise constraint on N_H along the line of sight to the central nucleus. These values are consistent with the idea that the X-ray emitter is buried more deeply within the dense material than are sur-

rounding dust shrouds responsible for the far-infrared emission.

The unification scheme of both types of Seyfert galaxies (Antonucci & Miller 1985) asserts that type 2 Seyferts contain a Seyfert 1 region hidden from our view behind a dusty torus. A handful of type 2 Seyfert galaxies have been found to have strongly absorbed X-ray continua (e.g., Awaki et al. 1990b; Awaki et al. 1991). According to this idea, the heavily obscured component of NGC 4945 can be explained by the Seyfert 2 model. Among the absorbing column densities measured in type 2 Seyferts, that of NGC 4945 is by far the largest.

4.2. *Scattered X-Rays from the Nucleus*

Since the previous observations of NGC 4945 in other wavelengths have suggested the nuclear starburst activities, we first discuss whether or not present X-ray results can be attributed to starburst activity. In starburst galaxies, X-rays are thought to be produced by free-free emission from the shock-heated gas arising from starburst activity. In the well-studied starburst galaxies, M82 (Fabbiano 1988; Tsuru et al. 1990) and NGC 3628 (Fabbiano, Heckman, & Keel 1990), diffuse X-ray emission having a temperature of several keV and being elongated along the minor axis of the galaxy disk have been found.

The hard X-ray component cannot be attributed to starburst activity, because it shows clear time variability in the short time scale of several hours. Also the ratio of hard X-rays relative to the infrared luminosity $\log (L_X/L_{IR}) \sim -2$ is much larger than the generic value of ~ 4 found in starburst galaxies (Heckman et al. 1990). Then, in order to investigate the possibility of a thermal origin for the soft X-ray component, we tried to fit the X-ray spectrum with a thermal bremsstrahlung model instead of power law for the soft component. We find that the soft X-ray component can be described by a thermal emission with a temperature of $kT = 13 \pm 6$ keV and luminosity of about 10^{40} ergs s^{-1} in the 2–10 keV band (see Table 3). These physical parameters are in the range of the "standard" starburst model (e.g., Mac Low & McCray 1988). In fact, *Ginga* observations of typical starburst galaxies find the temperature ranging 5–10 keV with luminosity of 10^{39}–10^{40} ergs s^{-1} (Ohashi et al. 1990). However, the iron energy of 6.5 ± 0.1 keV found in NGC 4945 is significantly lower than 6.7 keV which is predicted from optically thin hot gas with a temperature of several keV (Masai 1984). Also the observed equivalent width (~ 1.5 keV) is much larger than that observed from nearby starburst galaxies. In fact, the largest equivalent width of the iron measured in nearby starburst galaxies is about 200 eV (Ohashi et al. 1990). Moreover, it is larger than that expected from thin thermal emission (EW ~ 800 eV) assuming a temperature of $kT \sim 10$ keV and the solar abundance (Masai 1984). These suggest that the soft component is unlikely to be from starburst activity.

The energy of the iron emission of $E_{Fe} = 6.5 \pm 0.1$ keV and the large equivalent width of 1.5 ± 0.3 keV are consistent with those of the archetypical type 2 Seyfert galaxy NGC 1068 ($E_{Fe} = 6.55 \pm 0.1$ keV, EW $= 1.3 \pm 0.1$ keV, see Koyama et al. 1989). Although the continuum shape of the soft component has rather large ambiguity due to the contaminating source, the overall spectral shape below 10 keV is very similar to that of NGC 1068. The observed X-ray flux of NGC 1068 is interpreted to be the scattered nuclear light from the Seyfert 1 nucleus which is completely occulted from our direct view by an extremely large column $N_H > 10^{25}$cm^{-2}. Analogously we argue that the soft X-ray component of NGC 4945 can be attributed to the scattered X-rays.

As several authors have suggested, free electrons in ionized gas irradiated by the central source are likely scattering material (Antonucci & Miller 1985 and others). The two continuum components of the X-ray spectrum of NGC 4945 have similar spectral slopes to each other. This fact supports the scheme that the X-rays of the soft component are the scattered light by free electrons, since the electron scattering process has no dependence on the frequency. The lack of variability in the 4.5–9 keV band suggests that the iron line did not vary, since this line accounts for a significant amount of the emission in this band. This excludes that the iron line is produced near the continuum source.

Koyama (1992) and Mulchaey, Mushotzky, & Weaver (1992) have compared soft and hard X-ray fluxes from many type 2 Seyfert galaxies and reported that the luminosity of the scattered X-rays is several percent of the intrinsic X-rays. Similarly the luminosity ratio of the scattered (L_{sct}) to the direct (L_{true}) X-rays from NGC 4945 is found to be about 3%, and hence strengthen the occulting/scattering picture for NGC 4945. Heckman et al. (1990) found that $\Delta\Omega/4\pi$ is larger than 0.4 for the blowing fraction of the superwind associated with NGC 4945. If it is adopted for the opening fraction of the occulting torus, the electron scattering optical depth, τ_{es} is estimated to be equal or even smaller than 0.08, since $L_{sct}/L_{true} = (\Delta\Omega/4\pi)\tau_{es} \sim 0.03$. This figure is similar to the "illustrative" value of $\tau_{es} = 0.1$ or less found for NGC 1068 (Antonucci & Miller 1985; Miller, Goodrich, & Matthews 1991).

The line center energy of 6.5 ± 0.1 keV indicates the ionization states of iron ranging from neutral to Fe XXII. If the scattering is due to free electrons, iron and other elements are likely to be ionized. Thus the observed value of $N_H \sim 10^{22}$ cm^{-2} in the soft component would be due to the photoelectric absorption by cold gas located outside the X-ray scattering region. The observed Brα/Brγ emission line ratio of 5.6 ± 0.8 leads to $A_V = 13 \pm 3$ (Moorwood & Oliva 1988), which is consistent with the absorption of the soft X-ray component. The likely line width of 300–400 km s^{-1} for the observed Brackett lines (Moorwood & Oliva 1988) implies that they are produced in

TABLE 3

BEST-FIT PARAMETERS OF THERMAL EMISSION MODEL FOR THE SOFT COMPONENT

	HARD COMPONENT		SOFT COMPONENT			
MODEL	Photon Index	log N_H (H cm^{-2})	kT (keV)	log N_H (H cm^{-2})	E_{Fe} (keV)	REDUCED χ^2 (DOF)
(3).....	1.5 (0.3)	24.67 (0.04)	13 (6)	22 (1)	6.5 (0.1)	1.4 (29)

NOTE.—( ): Errors indicate 90% confidence level. Spectral fitting is performed in the 3–30 keV range by the following model: power-law model for the hard component and thermal bremsstrahlung model for the soft component. The contribution from the nearby contaminating source is also included in same way as Table 2.

the narrow line region (NLR). Therefore we suggest that the soft X-ray scattering region is, more or less, near the optical NLR.

5. CONCLUSIONS

1. The X-ray spectrum of NGC 4945 is found to be composed of three components: hard X-ray emission above 10 keV; a soft X-ray component seen below 10 keV; and iron emission line at about 6.5 keV.

2. The hard component exhibits a power-law spectrum with photon index of about 1.7 and large absorption having column density of about $10^{24.7}$H cm^{-2}. The intrinsic X-ray luminosity is estimated to be 10^{42} ergs s^{-1}. Clear intensity variability with a time scale of several hours is found from the hard component.

3. The X-ray spectrum of the soft component can be fitted with a power-law model having nearly same photon index but luminosity of only 3% of the hard component. In contrast with the hard component, the soft X-ray component shows no time variability. We also find a strong iron line at an energy of 6.5 ± 0.1 keV with an equivalent width of 1.5 ± 0.3 keV.

4. These observational facts given in (1)–(3) are fully consistent with the unified Seyfert scenario.

The authors would like to express thanks to all the members of *Ginga* team and are grateful to Dr. K. Leighly for critical reading of the manuscript. They also thank Prof. K. Wakamatsu for his valuable comments. This work is supported by Grant-in-aid for Scientific Research. The data analysis was performed using the FACOM M380 and M770 computers of High Energy Physics Laboratory in Nagoya University.

REFERENCES

Ables, J. G., et al. 1987, MNRAS, 226, 157
Antonucci, R. R., & Miller, J. S. 1985, ApJ, 297, 621
Awaki, H. 1991, Ph.D. thesis, Nagoya University, Nagoya, Japan
Awaki, H., Koyama, K., Kunieda, H., Takano, S., Tawara, Y., & Ohashi, T. 1990a, ApJ, 366, 88
Awaki, H., Koyama, K., Kunieda, H., & Tawara, Y. 1990b, Nature, 346, 544
Awaki, H., Kunieda, H., Tawara, Y., & Koyama, K. 1991, PASJ, 43, L37
Baan, W. A. 1985, Nature, 315, 26
Bachelor, R. A., Jauncey, D. L., & Whiteoak, J. B. 1982, MNRAS, 200, 19
Barr, P., & Mushotzky, R. F. 1986, Nature, 320, 421
Brock, D., Joy, M., Lester, D. F., Harvey, P. M., & Benton Elis, H., Jr, 1988 ApJ, 329, 208
dos Santos, P. M., & Lepine, J. R. D. 1979, Nature, 278, 34
Fabbiano, G. 1988, ApJ, 330, 672
Fabbiano, G., Heckman, T. M., & Keel, W. C. 1990, ApJ, 355, 442
Gardner, F. F., & Whiteoak, J. B. 1974, Nature, 247, 526
Harnett, J. I., & Reynolds, J. E. 1985, MNRAS, 215, 247
Hayashida, K., et al. 1989, PASJ, 41, 373
Heckman, T. M., Beckwith, S., Blitz, L., Skrutskie, M., & Ridgway, A. S. 1986, ApJ, 305, 278
Heckman, T. M., Armus, L., & Miley, G. K. 1990, ApJS, 74, 869
Kawara, K., Nishida, M., & Gregory, B. 1990, ApJ, 352, 433
Koyama, K. 1992, in Proc. X-Ray Emission from Active Galactic Nuclei and the Cosmic X-Ray Background, ed. W. Brinkman & J. Trumper, (MPE rep. 235), 74
Koyama, K., Inoue, H., Tanaka, Y., Awaki, H., Takano, S., Ohashi, T., & Matsuoka, M. 1989, PASJ, 41, 731
Mac Low, M., & McCray, R. 1988, ApJ, 324, 776
Masai, K. 1984, A&SS, 98, 367
Miller, J. S., Goodrich, R. W., & Mathews, W. G. 1991, ApJ, 378, 47
Moorwood, A. F. M., & Glass, I. S. 1984, A&A, 135, 281
Moorwood, A. F. M., & Oliva, E. 1988, A&A, 203, 278
Morrison, R., & McCammon, D. 1983, ApJ, 270, 119
Mulchaey, J. S., Mushotzky, R. F., & Weaver, K. A. 1992, ApJ, 390, L69
Mushotzky, R. F. 1982, ApJ, 256, 92
Nakai, N. 1989, PASJ, 41, 1107
Ohashi, T., Makishima, K., Tsuru, T., Takano, S., Koyama, K., & Stewart, G. C. 1990, ApJ, 365, 180
Phillips, M. M., Charles, P. A., & Baldwin, J. A. 1983, ApJ, 266, 485
Rice, W. A., et al. 1988, ApJS, 68, 91
Rothschild, R. E., Mushotzky, R. F., Baity, W. A., Gruber, D. E., Matteson, J. L., & Primini, F. A. 1983, ApJ, 269, 423
Tsuru, T., Ohashi, T., Makishima, K., Mihara, T., & Kondo, H. 1990, PASJ, 42, L75
Turner, M. J. L., et al. 1989, PASJ, 41, 345
Weedman, D. W., Feldman, F. R., Balzano, V. A., & Ramsey, L. W. 1981, ApJ, 248, 105
Whiteoak, J. B., & Gardner, F. F. 1973, Astrophys. Lett., 15, 211
———. 1976, Proc. Astron. Soc. Australia, 3, 71
———. 1977, Australian J. Physics, 30, 187
———. 1979, Proc. Astron. Soc. Australia, 3, 5
———. 1986, MNRAS, 222, 513
Wood, K. S., et al. 1984, ApJS, 56, 507